Anisotropic microwave propagation in a reconfigurable chiral spin soliton lattice

Y. Shimamoto [1,*] F. J. T. Goncalves,[2] T. Sogo,[1] Y. Kousaka,[1] and Y. Togawa [1]

[1]*Department of Physics and Electronics, Osaka Prefecture University, 1-1 Gakuencho, Sakai, Osaka 599-8531, Japan*
[2]*Helmholtz-Zentrum Dresden-Rossendorf, Institute of Ion Beam Physics and Materials Research,*
Bautzner Landstraße 400, 01328 Dresden, Germany

We investigated microwave propagation in the chiral spin soliton lattice (CSL) phase of micrometer-sized crystals of the monoaxial chiral helimagnet $CrNb_3S_6$. An advantage of the CSL is that its periodicity can be reconfigured over a macroscopic length scale by means of an external magnetic field. Using a two-antenna microwave spectroscopy technique, we measured the anisotropic response of the transmitted microwaves via the spin dynamics of the CSL. When propagating along the direction parallel to the helical axis, the microwave amplitude increased up to a factor of twenty with decreasing the number of chiral soliton kinks. When the propagation direction was rotated by 90° with regards to the helical axis, the microwave amplitude increased by one order of magnitude upon formation of the chiral helimagnetic order in the vicinity of zero magnetic field, exceeding that of the ferromagnetic phase above the critical field. Our findings open a novel route for controlling the characteristics of microwave propagation using noncollinear spin textures.

I. INTRODUCTION

Microwaves can propagate in magnetic materials via spin dynamic excitations. Recently, the excitation of spin waves in ferromagnetic systems has attracted much interest for device applications aiming at information transfer [1] and processing [2,3] without a loss of Joule heat. The ability to manipulate the amplitude, frequency, phase, and propagation direction of the spin waves may provide extended functionality of spin-wave based devices. A promising approach in order to enrich controllability of the microwave transmission characteristics is the use of reconfigurable noncollinear spin textures, such as the chiral spin soliton lattice (CSL) [4,5], magnetic domain walls [6] and magnetic skyrmions [7–9]. In particular, the CSL has the ability to vary the number of chiral soliton kinks (2π magnetic kinks) with a phase coherence over a macroscopic length scale, which can be seen as a way to control the characteristics of the microwave propagation [10].

Antisymmetric exchange interaction, frequently referred to as the Dzalloshinskii-Moriya (DM) interaction, is a key element in the formation of chiral magnetic textures in chiral magnetic materials [11,12]. The DM interaction competes with Heisenberg symmetric exchange interaction, resulting in the stabilization of the chiral helimagnetic order (CHM) at zero magnetic field. In the case of the prototype monoaxial chiral helimagnet $CrNb_3S_6$, the CHM emerges as a harmonic order below a critical temperature T_c of 127 K [13]. The period of the CHM in the $CrNb_3S_6$ was found to be 48 nm by Lorentz microscopy [5]. In the presence of an external magnetic field H, applied in a direction perpendicular to the principal axis of the crystal (c axis), the CHM turns into the nonlinear CSL, which consists of an array of chiral soliton kinks periodically partitioned by ferromagnetic domains, as illustrated in

Fig. 1(a). The period of the CSL increases depending on the strength of H below a critical field H_c. The number of chiral soliton kinks in specimens, namely a soliton density, becomes an order parameter, as it governs the process of CSL formation [5]. Finally, the CSL is completely saturated and transforms to a forced-ferromagnetic (F-FM) phase above H_c.

Given the unidirectional symmetry of the CSL and CHM one expects microwave transmission characteristics to depend on whether the propagation wave vector (k) of the spin excitations is along the direction parallel or perpendicular to the helical axis (c axis), as illustrated in Fig. 1(a). This expectation is supported by previous experimental and theoretical works in which uniform excitation modes were examined for both excitation configurations [14–17]. Indeed, it was found that the field dependence of the magnetic resonance frequency was sensitive to the direction of the driving microwave field relative to the c axis. In this respect, the anisotropic response of propagating microwaves with nonzero wave vector is very interesting.

In this manuscript, we investigate the transmission of microwave signals via the spin dynamics in micrometer-sized $CrNb_3S_6$ crystals, using a propagating spin wave spectroscopy technique. The amplitude of the microwave transmission strongly depends on the direction of the wave vector k relative to the c axis of the crystal as well as the strength of H. It is found that, in the configuration of k being parallel to the c axis, the microwave amplitude increases gradually, up to a factor of about twenty with increasing the strength of H, suggesting that the microwave propagation becomes more efficient with decreasing the number of chiral soliton kinks in the CSL. When microwave signals propagate in the direction perpendicular to the c axis, the appearance of the CSL attenuates the microwave transmission, with the exception of the behavior in the zero magnetic field region. After passing through zero magnetic field and being at magnetic fields lower than 10 mT,
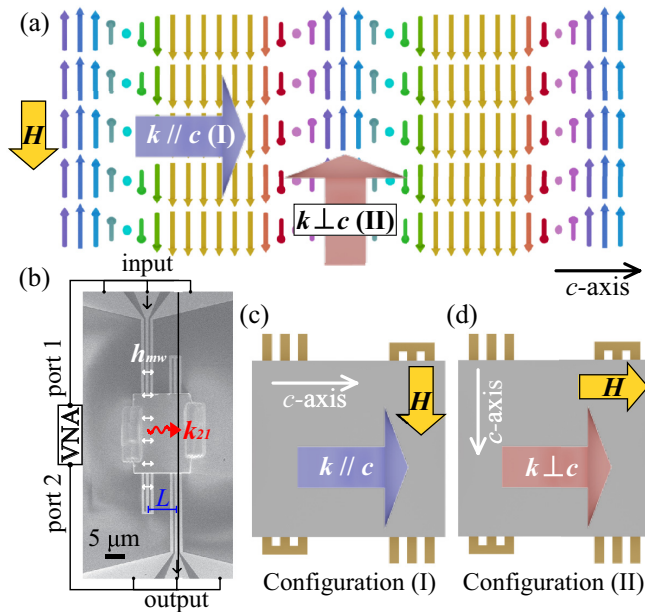
*y-shimamoto-spin@pe.osakafu-u.ac.jp

FIG. 1. (a) Schematic illustration of the chiral spin soliton lattice (CSL). An external magnetic field H is applied in the direction perpendicular to the helical axis of the CSL, corresponding to the c axis of the $CrNb_3S_6$ crystals. The microwave transmission properties were investigated in two configurations—the propagation wave vector k is parallel or perpendicular to the c axis. (b) SEM image of the antennas and micrometer-sized $CrNb_3S_6$ platelet. The microwave magnetic field h_{mw} is generated from port 1 of a vector network analyzer (VNA) and excites the spin system in the crystal. The microwave signals with a certain wave vector k are expected to propagate in the crystal over a distance L. The transmitted signals are picked up by the other antenna connecting to the port 2 of the VNA. Such a microwave propagation path in the sample is expressed as k_{21}. (c) and (d) Schematic illustrations of device configuration for the microwave propagation in the directions parallel (c) and perpendicular (d) to the c axis. The direction of H is set perpendicular to the c axis in each configuration. Dimensions of the specimen are 14.2 μm (along to the c axis), 20.0 μm (perpendicular to the c axis) and thickness of 1.15 μm in the k // c configuration. The distance between the center of the antennas L is 7 μm. In the $k \perp c$ configuration, dimensions are 20.2 μm (along to the c axis), 16.0 μm (perpendicular to the c axis), thickness of 650 nm. Propagation distance L is 9 μm.

where the CHM without any defect is supposed to exist, the microwave signals increase by about nine times in amplitude, compared to that observed at different magnetic fields within the CSL phase. The microwave amplitude at the CHM state exceeded that of the F-FM phase.

This manuscript is organized as follows. In Sec. II, we describe experimental methods and sample configuration. In Sec. III, we present the experimental findings of the microwave propagation in the CHM, CSL and F-FM states. The discussion and perspective on the results are given in Sec. IV.

II. METHOD AND DEVICE CONFIGURATION

An all-electrical detection method, also called propagating spin wave spectroscopy (PSWS) [18], was used to detect the microwave propagation through the micrometer-sized

crystal. Two shorted coplanar waveguides (CPWs), which consist 200 nm thick Au and work as antennas for the excitation (input) and detection (output) of the spin waves, were fabricated on an Al_2O_3 substrate using electron beam lithography. In the geometry employed here, signal and ground lines of 650 nm in width are separated by the gap of 600 nm. The ground-signal-ground geometry is such that the microwave fields are confined within the antennas and couple inductively to the spin system in the crystal placed above the CPWs. The in-plane component of the microwave fields h_{mw} dominantly excites the spin-wave propagation in the direction parallel to h_{mw} [18], as shown in Fig. 1(b). The nonzero microwave signals were measured at the second antenna inductively, at a distance L from the excitation antenna. The excitation range of wave vectors is determined by the dimensions of the CPWs, with the wave vectors k being in the direction parallel to the film plane, and perpendicular to the long axis of the antennas [18]. Using a microwave simulation package and by applying a Fourier transform to the spatial distribution of the microwaves, the excitation spectrum of the antenna was estimated. The resulting spectrum contains three wave vectors, a dominant wave vector at $k = 8.0$ and two weaker peaks at $k = 2.7$ and 13.0 μm^{-1}, all of which correspond to the wave number regime in which magnetic dipolar interactions dominate over exchange interactions [19].

Bulk single crystals of $CrNb_3S_6$ were grown using a chemical vapor transport method [20]. Micrometer-sized platelets of the crystal were cut from the bulk crystal using a focused ion beam method and placed at the center of the antennas. Figure 1(b) shows a scanning electron microscopy (SEM) image of the experimental device. The propagation properties in the configuration of k // c [configuration (I)] and $k \perp c$ [configuration (II)] were tested separately, as illustrated in Figs. 1(c) and 1(d), respectively. Experimentally, the main difference in the samples is that the c axis is rotated by 90 degrees with regards to the symmetry of the antennas. The direction of H is set in order to be always perpendicular to the c axis, allowing the CSL formation in both configurations.

It is known that magnetostatic (MS) modes are excited in magnetically saturated thin films at sufficiently large magnetic fields. The type of MS modes is determined by the relative direction between the propagation wave vector k and H. In an in-plane magnetized film, magnetostatic surface waves (MSSW) are excited when $k \perp H$ [21,23]. While magnetostatic backward volume waves (MSBVW) appear when k // H [22,23]. These MS modes have different dispersion relation, thus resulting in a nonreciprocal response in signal amplitude [21–23]. In the present study, the F-FM phase is expected to exhibit the MSSW mode in the configuration (I) and the MSBVW mode in the configuration (II). However, owing to the presence of the CSL and CHM states in the field regime below H_c, one expects distinct microwave propagation characteristics.

The microwave circuit is connected to a two-port vector network analyzer (VNA), where one port is the emitter and the other port is the receiver. A transmission parameter S was measured by the VNA as a function of the frequency at various magnetic fields. In the process of the data analysis, the spin-wave spectra ΔS were obtained after subtracting a background spectrum from the raw data in order to remove
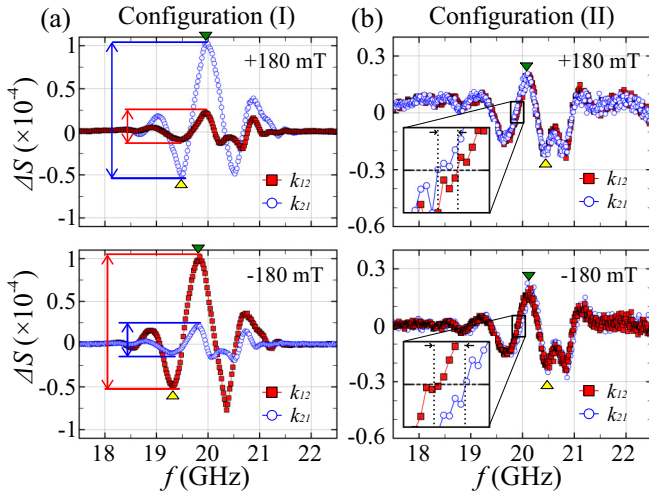
FIG. 2. Line traces of ΔS for the positive and negative propagation directions in the F-FM phase for the configuration (I)-(a) and configuration (II)-(b). The value of $\mu_0 H$ is $+180$ and -180 mT for the top and bottom panels, respectively. The amplitude differences between the signals corresponding to k_{21} and k_{12} are indicated by the vertical blue and red arrows, respectively. The insets in (b) show a zoom-in view of the frequency difference between the k_{21} and k_{12} waves. Upward triangles and downward triangles indicate the peaks, which are used for evaluating the magnetic field dependence of the frequency and amplitude shown in the Fig. 4.
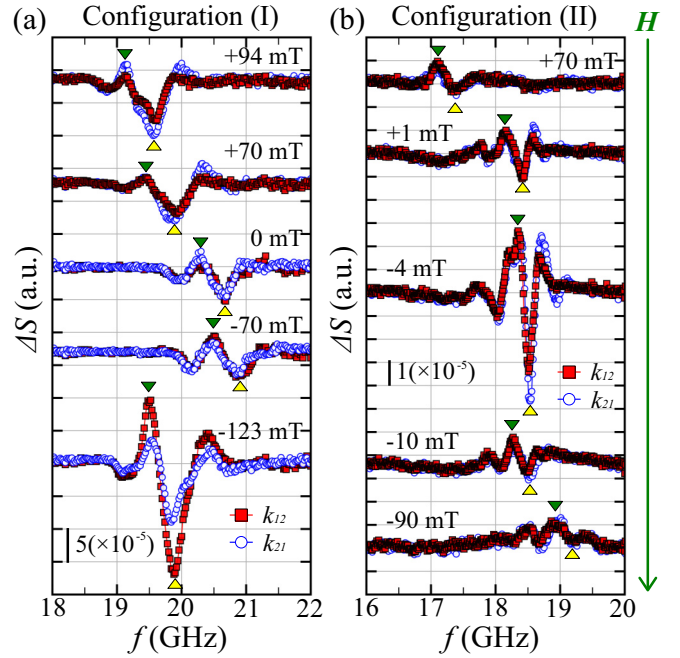

FIG. 3. Microwave transmission spectra of the CSL phase at different magnetic fields, in the configuration (I)-(a) and (II)-(b). The scale bar indicates the amplitude of ΔS. The magnetic field was swept from top (positive H) to bottom (negative H) as indicated by green arrow on the right.

unwanted nonmagnetic losses of the circuit. The microwave transmission form the port 1 to port 2 of the VNA corresponds the forward propagation path of spin-wave signals k_{21} and the reverse propagation path is expressed as k_{12}. The microwave transmission measurements were performed at a temperature of 20 K in the present study.

III. EXPERIMENTAL RESULTS

First, let us see the behavior of the spin wave propagation in the F-FM state. Figure 2(a) shows ΔS spectra for the positive and negative propagation directions in the configuration (I). The magnitude of H was set to 180 mT, while its direction was switched to observe any nonreciprocal characteristics. The spectra exhibit amplitude oscillations irrespective of the propagation direction. This oscillatory behavior is caused by a continuous phase variation of spin waves over the distance between the excitation and detection antennas, as is typically observed in the spin-wave spectra of conventional ferromagnetic thin films [18].

Noticeably, the ΔS amplitude for k_{21} wave was about three times larger than that for k_{12} wave at $+180$ mT. When the polarity of H was reversed, the ΔS spectra for k_{21} and k_{12} swapped their waveforms, as shown in the bottom panel of Fig. 2(a). Such a difference in the amplitude in the F-FM state for (I) is characteristic for MSSW modes [21,23]. In line with the MSSW theory, the microwaves are bound to the surface of the metallic specimen due to the finite penetration depth caused by the skin depth in the gigahertz frequency range. Thus the spin wave propagation occurs predominantly at the top or bottom surfaces of the micrometer-sized crystal, depending on the signs of k and H. The efficiency of the

spin excitation differs from the top and bottom interfaces because the dynamic magnetic fields decay exponentially from the bottom surface of the platelet. Therefore the amplitude asymmetry of counter propagating spin waves appears in the MSSW configuration [21,23].

Figure 2(b) shows the spin wave propagation in the F-FM state for the configuration (II). The amplitude of the microwave signals is three times smaller than that for (I). The counter propagating waves exhibit a similar waveform. However, they are shifted in frequency by approximately 50 MHz, as highlighted in the inset of Fig. 2(b). This feature contrasts with the observations in (I), where only amplitude asymmetry between k_{21} and k_{12} waves was observed.

The reduced amplitude, as well as the absence of the amplitude nonreciprocity found in (II) are consistent with the behavior expected for the MSBVW mode. In this case, the microwaves propagate as a volume wave throughout the specimen and thus nonreciprocal response due to geometrical asymmetry of the microwave circuit does not occur. Therefore the nonreciprocity in frequency observed in the spin wave propagations is directly ascribed to the intrinsic properties of the material. Note that nonreciprocal transport occurs in chiral materials when the magnetic field is applied parallel to an electric current flow, in what is frequently referred to as a magnetochiral effect [24]. The magnetochiral effect in the $CrNb_3S_6$ was detected via electrical transport [25]. Such magnetochiral nonreciprocity is also induced in the spin wave propagation in chiral magnetic materials [26–29]. The presence of the k-linear term in the magnon dispersion, originating from the DM interaction, gives nonreciprocal properties of the spin wave propagation. In principle, the frequency shift
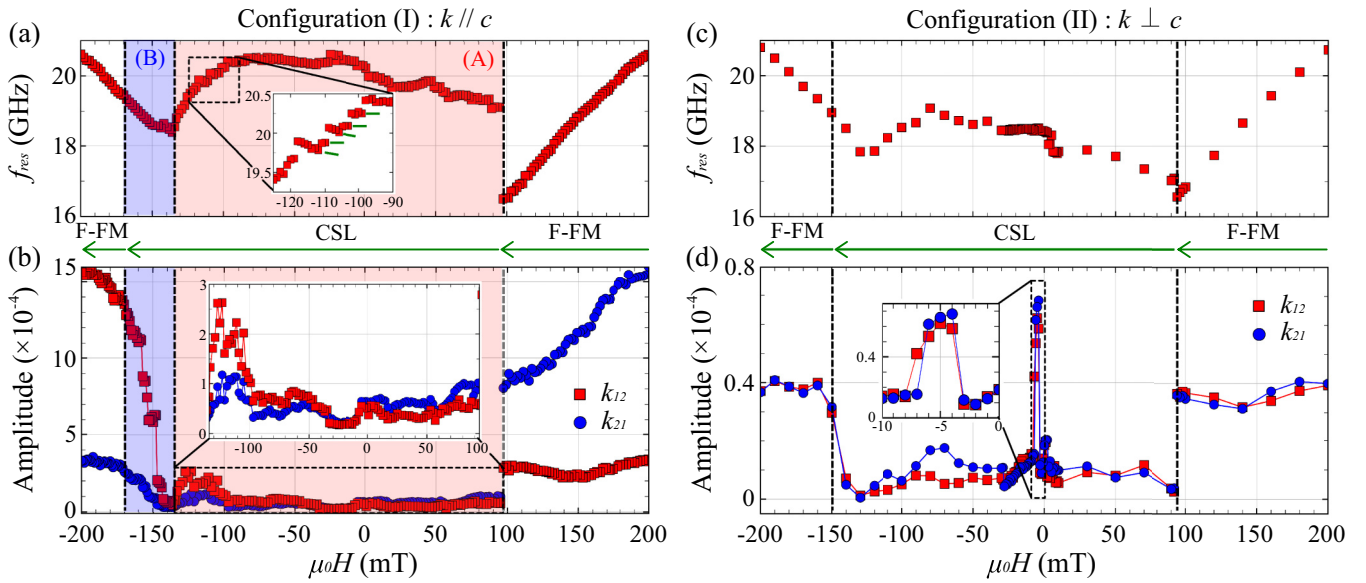
FIG. 4. Field dependence of the frequency (top) and amplitude (bottom) of microwave propagation in configuration (I) and (II). The magnetic field was swept from positive to negative values, as illustrated by the green arrows. Frequency data are extracted from the spectra shown in Figs. 2 and 3, indicated by the downward triangles. Horizontal green lines in inset (a) indicate the discrete changes in the frequency of the microwave signals. The amplitude is defined as the difference between the local maxima and minima of the ΔS in the microwave transmission spectra, illustrated in Figs. 2 and 3 by the upward and downward triangles, respectively.

observed in (II) in our measurements should have the same origin as that observed in other chiral magnetic materials. However, the measurements of the microwave propagation using the $CrNb_3S_6$ crystals with opposite handedness are required to confirm the origin of the frequency shift observed in this study as the magnetochiral effect.

Next, let us discuss the microwave propagation in the CSL phase. Figure 3(a) shows the microwave transmission spectra in the CSL phase in the configuration (I). The spectra obtained in the configuration (II) are presented in Fig. 3(b). In (I), the low-field region shows no significant difference in the spectra when comparing the propagation directions k_{21} and k_{12}. However, at larger values of H, concurrent with a lower number of chiral soliton kinks in the CSL, the amplitude and amplitude nonreciprocity become more pronounced.

In the configuration (II), a comparatively large microwave signal is found at -4 mT, corresponding to the CHM state, as shown in Fig. 3(b). However, the microwave amplitude is suddenly and largely suppressed with increasing the H strength, which contrasts with the results for (I) shown in Fig. 3(a).

Figure 4 shows a summary of the field dependence of the frequency and amplitude of the microwave propagation in (I) and (II). The values of the microwave amplitude were evaluated by subtracting the local maxima and minima of each spectrum, indicated respectively by the upward and downward triangles shown in Figs. 2 and 3.

Note that the process of the CSL formation is strongly influenced by the sweep direction of H in the micrometer-sized samples [14,30,31]. In this study, H was varied from $+200$ mT to -200 mT at a fixed temperature. The CSL phase appeared at a field H_{jump} of $+94$ mT in the positive H regime, while the F-FM state was formed at the H_c of -170 mT in the negative H regime in (I). In configuration (II), H_{jump} was $+92$ mT, while H_c was -150 mT. During field decreasing

process from the F-FM state to CSL phase, the chiral soliton kinks need to overcome the surface barrier in order to penetrate into the platelet [30]. As a consequence, the transformation into the CSL phase occurs at the field strength lower than H_c and many magnetic dislocations are nucleated in the CSL [17,32]. Such magnetic dislocations are vanishing with reducing the magnetic field toward zero. Eventually, the ideal CHM without magnetic defect emerges after passing through zero field [17,32]. In the process of further increasing H, the ideal CHM transforms into the CSL, which also contains no magnetic dislocations, and turns into the F-FM state at H_c. In consequence, the properties of the microwave propagation in the CSL phase show asymmetric response with regard to zero magnetic field.

The frequency of the resonance modes in the F-FM phase shows a linear increase with increasing the absolute value of H for both (I) and (II), as shown in Figs. 4(a) and 4(c), respectively. This behavior is consistent with MS modes [21–23]. In the CSL phase, we focus on the behavior in the negative H regime, where the ideal CSL is supposed to exist. The data corresponding to (I) presented in Fig. 4(a) shows that the frequency of the microwave transmission increases slightly from 20 to 20.5 GHz as the field increases from 0 to -84 mT. Between -84 and -136 mT, the frequency decreases more rapidly from 20.5 to 18.3 GHz. In this field range, stepwise behavior of the microwave frequency was observed due to discrete changes in the number of chiral soliton kinks, as highlighted in the inset. Thus the decrease in the frequency correlates to the decrease in the number of chiral soliton kinks in the CSL. The domelike profile of the frequency and the stepwise behavior observed in the field region between 0 and -136 mT [region (A)] are similar to those of the resonance frequency obtained in the magnetic resonance measurements [14,15], where the excitation field is parallel to the c axis
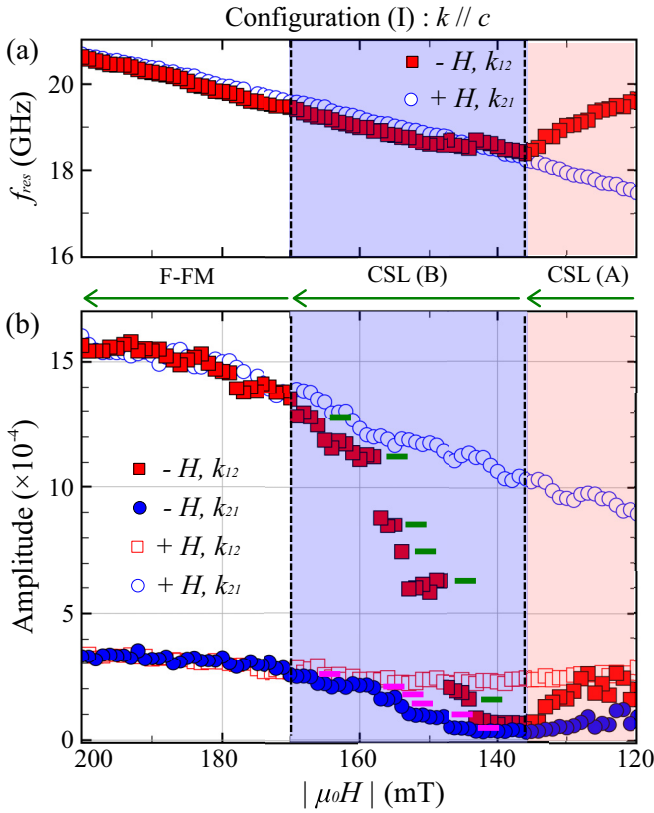
FIG. 5. (a) Frequency of the microwave propagation for k_{12} wave at $-H$ (field increasing process) and k_{21} wave at $+H$ (field decreasing process) as function of the absolute value of H in (I). (b) Microwave amplitude of k_{12} and k_{21} waves for both positive and negative H in (I). Horizontal green and pink lines indicate the position of the discrete changes in the amplitude. Green arrows indicate the H sweep direction for the data of the field increasing process, indicated by solid markers.

of the $CrNb_3S_6$ crystal. Recently, the resonance modes observed in the micrometer-sized systems, where the spins at the edges are pinned, are ascribed to the collective dynamics of the CSL by an analytical theory and numerical simulations [16]. Therefore our experimental observations support that the mode originated from the collective dynamics of the CSL was excited in the microwave propagation measurements. Just within the H region between -136 and -170 mT below H_c indicated in blue, as region (B), the frequency of the microwave transmission increases with increasing the strength of H in spite of the CSL phase. Later, we discuss the behavior observed in the region (B).

Recent experimental work presented in Ref. [14], the resonance mode was split into two in a configuration where the excitation field is perpendicular to the c axis, which is equivalent to configuration (II) in the present work. However, in the microwave propagation experiments, only the mode at lower frequency was observed in (II), as shown in Fig. 4(c). The higher frequency mode could not be detected, possibly due to its weak amplitude.

The amplitude variation of the microwave transmission in the CSL phase exhibits interesting behavior. In (I), an increase of the microwave amplitude is found with increasing the

strength of H in the region (A) of the CSL phase, as seen in the inset of Fig. 4(b). For instance, the microwave amplitude of k_{12} wave changes from ΔS of 0.15×10^{-4} to 2.63×10^{-4} in the negative H regime. Furthermore, when comparing the amplitude and frequency of the microwave transmission in the negative H regime, the increase of the amplitude seems to occur in the field range where a decrease of the frequency is also observed. This behavior indicates that the number of chiral soliton kinks is likely to correlate with the amplitude of the microwave transmission. Therefore the microwave propagation becomes more efficient with reducing the density of chiral soliton kinks in the configuration where the microwave propagation is parallel to the c axis of the crystal.

Figures 5(a) and 5(b) show the frequency and amplitude of k_{12} and k_{21} waves for both the negative H (field increasing process) and positive H (field decreasing process) as function of the absolute value of H in (I). Here we identify the phase transition from the CSL to F-FM phase in the field increasing process based on the spin dynamic properties.

Note that, in the MSSW theory, the spin wave amplitude for k_{12} wave at $-H$ ($+H$) is equal to that for k_{21} wave at $+H$ ($-H$) [21,23]. Thus the existence of the F-FM phase can be seen by comparing the amplitude of counter propagating microwaves at the same magnitude of H and opposite polarity. Upon decreasing the strength of H, the supersaturated F-FM state exists down to 94 mT (H_{jump}) [30,31], as indicated by the open symbols in Fig. 5. Therefore, in the present sample, the complete phase transition from the CSL to F-FM phase occurs at 170 mT (H_c), where the microwave amplitude of the field increasing process begins to overlap with that of the field decreasing process.

The difference between the (A) and (B) regimes of the CSL phase is the field dependence of the frequency of the microwave propagation. In Fig. 5(a), the microwave frequency for the field increasing process decreases with increasing the H in the regime (A), which is the characteristics for the excitation of the collective dynamics of the CSL [14–16]. On the other hand, in (B), the linear increase of the microwave frequency was found, which is the characteristics for the excitation of the MS mode. Indeed, the discrete increase of the microwave amplitude with increasing the strength of H was observed in (B), as shown in Fig. 5(b), which is the strong evidence for being the CSL phase. These observations suggest that, just near the H_c, the microwave propagation linked to collective dynamics of the CSL progressed towards that of MS mode in the F-FM phase, as the number of the chiral soliton kinks tends to zero.

In the configuration (II), where the microwave propagates along the plane of the CSL, it appears that the number of chiral soliton kinks does not affect the microwave propagation in the same manner as found in (I). A striking feature of the microwave propagation for (II) is an enhancement of the microwave amplitude within a narrow field window between -4 and -7 mT, as shown in Fig. 4(d). Surprisingly, the microwave amplitude increases by a factor of about nine compared to that at other field values in the CSL phase and goes beyond that of the F-FM phase. Namely, the enhancement of the microwave amplitude appears to be concurrent with the emergence of the ideal CHM without any defects [17,32]. However, the transformation from harmonic CHM to

nonlinear CSL immediately attenuates the microwave transmission. The experimentally observed enhancement of the microwave amplitude at the CHM state has not yet been identified in the analytical and numerical investigations. Further investigations, in terms of both the experiment and theory, are necessary to clarify the mechanism.

IV. DISCUSSION AND PERSPECTIVE

In this paper, we described the anisotropic behavior of the microwave propagation via the collective dynamics of the chiral magnetic orders found in micrometer-sized crystals of $CrNb_3S_6$. The number of chiral soliton kinks in the CSL plays a key role in controlling the amplitude of the microwave propagation in the configuration (I), owing to the existence of the chiral soliton kinks which act as obstacles to the microwave propagation. On the other hand, in the configuration (II), the amplitude of the propagating signals was enhanced at the CHM state, where the chiral soliton kinks is dense. This behavior contrasts with the observations in (I), highlighting the asymmetric behavior of the microwave propagation in the CHM and CSL.

Several numerical [33,34] and experimental studies [35–38] have reported amplitude attenuation of spin waves passing through the single magnetic domain wall (DW). Geometrically, each of chiral soliton kinks is consistent with the 2π DW. When each chiral soliton kink is far apart and decoupled from the neighboring kinks, it is expected that the collective dynamics of the CSL does not occur and the MS mode propagates through isolated chiral soliton kinks. Therefore, in the region (B) of CSL phase in (I), the chiral soliton kinks may behave as the magnetic DWs and work as attenuators for the microwave propagation. However, it is not easy to realize the gradual changes of the propagation properties by varying the number of the DWs in conventional magnetic systems.

From a technological viewpoint, the asymmetric behavior observed in the CHM and CSL may add a unique degree of controllability of the microwave propagation. The CHM works as a good transmission line for microwave propagation in (II). Indeed, the enhanced signals at the ideal CHM state exceed those in the F-FM state. As a consequence, just in the CHM state, the microwave amplitude in (II) is larger than that in (I). These features suggest that the CHM and CSL have the possibility to rotate the dominant propagation direction of microwave signals by interchanging the spin textures. Thus the unique controllability of the CSL is useful for manipulating the direction of the microwave propagation in addition to the amplitude and frequency.

ACKNOWLEDGMENTS

[1] Y. Kajiwara, K. Harii, S. Takahashi, J. Ohe, K. Uchida, M. Mizuguchi, H. Umezawa, H. Kawai, K. Ando, K. Takanashi, S. Maekawa, and E. Saitoh, Transmission of electrical signals by spin-wave interconversion in a magnetic insulator, Nature (London) **464**, 262 (2010).

[2] A. V. Chumak, V. I. Vasyuchka, A. A. Serga, and B. Hillebrands, Magnon spintronics, Nat. Phys. **11**, 453 (2015).

[3] T. Schneidera, A. A. Serga, B. Leven, B. Hillebrands, R. L. Stamps, and M. P. Kostylev, Realization of spin-wave logic gates, Appl. Phys. Lett. **92**, 022505 (2008).

[4] I. E. Dzyaloshinsky, Theory of helicoidal structures in antiferromagnets. I. Nonmetals, Sov. Phys. JETP **19**, 960 (1964).

[5] Y. Togawa, T. Koyama, K. Takayanagi, S. Mori, Y. Kousaka, J. Akimitsu, S. Nishihara, K. Inoue, A. S. Ovchinnikov, and J. Kishine, Chiral Magnetic Soliton Lattice on Chiral Helimagnet, Phys. Rev. Lett. **108**, 107202 (2012).

[6] A. Hubert and R. Schäfer, *Magnetic Domains: The Analysis of Magnetic Microstructures* (Springer-Verlag, Berlin, Heidelberg, 1998).

[7] A. N. Bogdanov and D. A. Yablonskii, Thermodynamically stable "vortices" in magnetically ordered crystals. The mixed state of magnets, Sov. Phys. JETP **68**, 101 (1989).

[8] S. Mühlbauer, B. Binz, F. Jonietz, C. Pfleiderer, A. Rosch, A. Neubauer, R. Georgii, and P. Böni, Skyrmion lattice in a chiral magnet, Science **323**, 915 (2009).

[9] X. Z. Yu, Y. Onose, N. Kanazawa, J. H. Park, J. H. Han, Y. Matsui, N. Nagaosa, and Y. Tokura, Real-space observation of a two-dimensional skyrmion crystal, Nature (London) **465**, 901 (2010).

[10] Y. Shimamoto, F. J. T. Goncalves, T. Sogo, Y. Kousaka, and Y. Togawa, Switching behavior of the magnetic resonance in a monoaxial chiral magnetic crystal $CrNb_3S_6$, Appl. Phys. Lett. **115**, 242401 (2019).

[11] I. E. Dzyaloshinsky, A thermodynamic theory of "weak" ferromagnetism of antiferromagnetics, J. Phys. Chem. Solids **4**, 241 (1958).

[12] T. Moriya, Anisotropic superexchange interaction and weak ferromagnetism, Phys. Rev. **120**, 91 (1960).

[13] T. Miyadai, K. Kikuchi, H. Kondo, S. Sakka, M. Arai, and Y. Ishikawa, Magnetic properties of $Cr_{1/3}NbS_2$, J. Phys. Soc. Jpn. **52**, 1394 (1983).

[14] F. J. T. Goncalves, T. Sogo, Y. Shimamoto, Y. Kousaka, J. Akimitsu, S. Nishihara, K. Inoue, D. Yoshizawa, M. Hagiwara, M. Mito, R. L. Stamps, I. G. Bostrem, V. E. Sinitsyn, A. S. Ovchinnikov, J. Kishine, and Y. Togawa, Collective resonant

dynamics of the chiral spin soliton lattice in a monoaxial chiral magnetic crystal, Phys. Rev. B **95**, 104415 (2017).

[15] F. J. T. Goncalves, T. Sogo, Y. Shimamoto, I. Proskurin, V. E. Sinitsyn, Y. Kousaka, I. G. Bostrem, J. Kishine, A. S. Ovchinnikov, and Y. Togawa, Tailored resonance in micrometer-sized monoaxial chiral helimagnets, Phys. Rev. B **98**, 144407 (2018).

[16] J. Kishine, Vl. E. Sinitsyn, I. G. Bostrem, I. Proskurin, F. J. T. Goncalves, Y. Togawa, and A. S. Ovchinnikov, Theory of standing spin waves in a finite-size chiral spin soliton lattice, Phys. Rev. B **100**, 024411 (2019).

[17] F. J. T. Goncalves, Y. Shimamoto, T. Sogo, G. W. Paterson, Y. Kousaka, and Y. Togawa, Field driven recovery of the collective spin dynamics of the chiral soliton lattice, Appl. Phys. Lett. **116**, 012403 (2020).

[18] V. Vlaminck and M. Bailleul, Spin-wave transduction at the submicrometer scale: Experiment and modeling, Phys. Rev. B **81**, 014425 (2010).

[19] D. Stancil and A. Probhakar, *Spin Waves: Theory and Applications* (Springer, New York, 2009).

[20] Y. Kousaka, Y. Nakao, J. Kishine, M. Akita, K. Inoue, and J. Akimitsu, Chiral helimagnetism in $T_{1/3}NbS_2$ (T=Cr and Mn), Nucl. Instrum. Methods Phys. Res., Sect. A **600**, 250 (2009).

[21] R. Damon and J. Eshbach, Magnetostatic modes of a ferromagnet slab, J. Phys. Chem. Solids **19**, 308 (1961).

[22] R. Damon and H. Vaart, Propagation of magnetostatic spin waves at microwave frequencies in a normally-magnetized disk, J. Appl. Phys. **36**, 3453 (1965).

[23] J. P. Parekh, K. W. Chang, and H. S. Tuan, Propagation characteristics of magnetostatic waves, Circ. Syst. Signal Process. **4**, 9 (1985).

[24] G. L. J. A. Rikken, J. Fölling, and P. Wyder, Electrical Magnetochiral Anisotropy, Phys. Rev. Lett. **87**, 236602 (2001).

[25] R. Aoki, Y. Kousaka, and Y. Togawa, Anomalous Nonreciprocal Electrical Transport on Chiral Magnetic Order, Phys. Rev. Lett. **122**, 057206 (2019).

[26] Y. Iguchi, S. Uemura, K. Ueno, and Y. Onose, Nonreciprocal magnon propagation in a noncentrosymmetric ferromagnet $LiFe_5O_8$, Phys. Rev. B **92**, 184419 (2015).

[27] S. Seki, Y. Okamura, K. Kondou, K. Shibata, M. Kubota, R. Takagi, F. Kagawa, M. Kawasaki, G. Tatara, Y. Otani, and Y. Tokura, Magnetochiral nonreciprocity of volume spin wave propagation in chiral-lattice ferromagnets, Phys. Rev. B **93**, 235131 (2016).

[28] R. Takagi, D. Morikawa, K. Karube, N. Kanazawa, K. Shibata, G. Tatara, Y. Tokunaga, T. Arima, Y. Taguchi, Y. Tokura, and S. Seki, Spin-wave spectroscopy of the Dzyaloshinskii-Moriya interaction in room-temperature chiral magnets hosting skyrmions, Phys. Rev. B **95**, 220406(R) (2017).

[29] T. Weber, J. Waizner, G. S. Tucker, R. Georgii, M. Kugler, A. Bauer, C. Pfleiderer, M. Garst, and P. Böni, Field dependence of nonreciprocal magnons in chiral MnSi, Phys. Rev. B **97**, 224403 (2018).

[30] M. Shinozaki, Y. Masaki, R. Aoki, Y. Togawa, and Y. Kato, Intrinsic hysteresis due to the surface barrier for chiral solitons in monoaxial chiral helimagnets, Phys. Rev. B **97**, 214413 (2018).

[31] Y. Togawa, T. Koyama, Y. Nishimori, Y. Matsumoto, S. McVitie, D. McGrouther, R. L. Stamps, Y. Kousaka, J. Akimitsu, S. Nishihara, K. Inoue, I. G. Bostrem, Vl. E. Sinitsyn, A. S. Ovchinnikov, and J. Kishine, Magnetic soliton confinement and discretization effects arising from macroscopic coherence in a chiral spin soliton lattice, Phys. Rev. B **92**, 220412(R) (2015).

[32] G. W. Paterson, T. Koyama, M. Shinozaki, Y. Masaki, F. J. T. Goncalves, Y. Shimamoto, T. Sogo, M. Nord, Y. Kousaka, Y. Kato, S. McVitie, and Y. Togawa, Order and disorder in the magnetization of the chiral crystal $CrNb_3S_6$, Phys. Rev. B **99**, 224429 (2019).

[33] J.-S. Kim, M. Stärk, M. Kläui, J. Yoon, C.-Y. Yoon, L. Lopez-Diaz, and E. Martinez, Interaction between propagating spin waves and domain walls on a ferromagnetic nanowire, Phys. Rev. B **85**, 174428 (2012).

[34] X. Wang, G. Guo, Y. Nie, G. Zhang, and Z. Li, Domain wall motion induced by the magnonic spin current, Phys. Rev. B **86**, 054445 (2012).

[35] P. Pirro, T. Koyama, T. Brächer, T. Sebastian, B. Leven, and B. Hillebrands, Experimental observation of the interaction of propagating spin waves with Néel domain walls in a Landau domain structure, Appl. Phys. Lett. **106**, 232405 (2015).

[36] S. J. Hämäläinen, M. Madami, H. Qin, G. Gubbiotti, and S. v. Dijken, Control of spin-wave transmission by a programmable domain wall, Nat. Commun. **9**, 4853 (2018).

[37] J. Han, P. Zhang, J. T. Hou, S. A. Siddiqui, and L. Liu, Mutual control of coherent spin waves and magnetic domain walls in a magnonic device, Science **366**, 1121 (2019).

[38] O. Wojewoda, T. Hula, L. Flajšman, M. Vaňatka, J. Gloss, J. Holobrádek, M. Staňo, S. Stienen, L. Körber, K. Schultheiss, M. Schmid, H. Schultheiss, and M. Urbánek, Propagation of spin waves through a Néel domain wall, Appl. Phys. Lett. **117**, 022405 (2020).